

## A NOVEL LESS DISSIPATION FINITE-DIFFERENCE LATTICE BOLTZMANN SCHEME FOR COMPRESSIBLE FLOWS

Q. CHEN and X. B. ZHANG\*

*School of Energy and Power Engineering  
Nanjing University of Science and Technology  
Jiangsu 210094, P. R. China  
\*zhangxb680504@163.com*

Received 10 November 2011

Accepted 14 August 2012

Published 19 October 2012

In this paper, a new smoothness indicator is proposed to improve the finite-difference lattice Boltzmann method (FDLBM). The necessary and sufficient conditions for convergence are derived. A detailed analysis reveals that the convergence order is higher than that of the previous finite-difference scheme. The coupled double distribution function (DDF) model is used to describe discontinuity flows and verify the improvement. Numerical simulations of compressible flows with shock wave show that the improved finite-difference lattice Boltzmann scheme is accurate and has less dissipation. The numerical results are found to be in good agreement with the analytical results and better than those of the previous scheme.

*Keywords:* Less dissipation; FDLBM; coupled DDF model; smoothness indicator; compressible flows.

PACS Nos.: 02.70.-c, 47.11.-j, 47.40.-x.

### 1. Introduction

In the past two decades, the lattice Boltzmann method (LBM), which originates from the lattice gas automata method, has developed into an alternative and promising numerical scheme for simulating fluid flows and modeling physics in fluids.<sup>1-5</sup> Unlike the conventional numerical methods, LBM simulates fluid flows by tracking the evolutions of the distribution functions and then accumulates the distributions to obtain macroscopic averaged properties. Because of its kinetic nature and distinctive computational features, LBM has received much attention in a variety of dynamic problems, such as multiphase/multicomponent flows, porous media flows, particulate suspensions flows, turbulence flows, magneto-hydrodynamics, etc.

\*Corresponding author.

Although the LBM has achieved great success in simulating nearly incompressible and isothermal flows, it has not been able to handle realistic thermal compressible flows with enough satisfaction.<sup>6</sup> Nevertheless, compressible flows with shocks play an important role in various field,<sup>7,8</sup> so it is necessary to study the compressible flows. To overcome this constraint, many compressible lattice Boltzmann models have been developed. These models can be classified into four approaches. First, it is the multi-speed approach.<sup>9–17</sup> The multispeed approach is a straightforward extension of the isothermal lattice Boltzmann models in which only the density distribution function is used. To recover the energy equation at the macroscopic level, additional particle speeds are needed and the equilibrium density distribution function should include higher-order velocity terms. The multispeed models usually suffer severe numerical instability and a narrow range of temperature variation. Moreover, the Prandtl number is usually fixed at constant and the specific-heat ratio cannot be chosen freely. Second, it includes various shock-capturing schemes based on the LBM for solving fully compressible Euler<sup>18–20</sup> or Navier–Stokes equations.<sup>21–23</sup> In this approach, the lattice velocities are chosen according to the local flow velocity and internal energy. Then the fluid velocity is no longer limited by the lattice velocities. Consequently, it permits the mean flow to have high Mach number. However, the relaxation time  $\tau$  is fixed and the Prandtl number is equal to the specific-heat ratio, which may limit its application. The third approach is the multiple-relaxation-time (MRT) approach, developed by Xu *et al.*<sup>24–27</sup> In this approach, the collision step is first calculated in the kinetic moment space. Then the streaming step is performed back in the discrete velocity space. Compared to the single-relaxation-time (SRT) approach, the MRT approach has more adjustable parameters and degrees of freedom, i.e. the relaxation rates of the various kinetic moments due to particle collisions can be adjusted independently. The fourth approach is double distribution function (DDF) approach, developed by He *et al.*<sup>6</sup> In this approach, a compressible LBM based on the DDF model<sup>28,29</sup> is established to obtain an adjustable specific-heat ratio and Prandtl number. An implicit–explicit FDLBM is adopted to capture the shock waves in compressible flows. The time derivative is calculated using the total variation diminishing (TVD) scheme. Spatial derivative in convection term  $e_\alpha \cdot \nabla f_\alpha$  is calculated using the fifth-order weighted essentially nonoscillatory (WENO) scheme. The numerical results show that the FDLBM together with DDF model can solve the compressible flows efficiently.

The FDLBM was developed by Reider and Sterling.<sup>30</sup> Later, Cao *et al.*<sup>31</sup> proposed to use a second-order Runge–Kutta scheme for time discretization and discussed the FDLBM in detail. Mei and Shyy<sup>32</sup> suggested a new FDLBM in curvilinear coordinates using body-fitted coordinates with nonuniform grids. The collision term was treated semi-implicitly to improve the numerical stability in their paper. Tolke *et al.*<sup>33</sup> discussed the implicit discretization and nonuniform mesh refinement approaches in the FDLBM and validated their approaches with steady flows. By introducing a novel distribution function, Guo *et al.*<sup>34</sup> obtained an explicit FDLBM for curvilinear coordinates. Li *et al.*<sup>35</sup> proposed an alternative FDLBM in body-fitted coordinates by employing the features of the implicit–explicit finite-difference

scheme. Moreover, the FDLBM was also used for simulating thermal flows,<sup>36</sup> fracture flows,<sup>37</sup> phase separation in liquid–vapor systems,<sup>38</sup> compressible flows with shock waves,<sup>39–42</sup> and binary mixtures.<sup>43,44</sup> In this work, a less dissipation FDLBM is proposed. In order to capture the discontinuities in compressible flows with sufficient accuracy, a new smoothness indicator is proposed by analyzing the space discretization. The convergence order is found to be higher than that of the previous finite-difference scheme. The numerical results demonstrate that the new FDLBM can solve compressible problems accurately and efficiently.

The rest of this paper is organized as follows. In Sec. 2, the FDLBM based on coupled DDF is described. In Sec. 3, the space discretization scheme WENO is analyzed and the improved scheme is proposed. The improved FDLBM is applied to compressible flows in Sec. 4. Finally, a brief conclusion is given in Sec. 5.

## 2. Coupled DDF of FDLBM

### 2.1. D2Q13 model

A lattice Boltzmann model has three main ingredients: discrete velocity model, the equilibrium density distributions and an evolution equation. In order to recover the compressible momentum equation correctly, the D2Q13 square lattice model (see in Fig. 1) is used which is defined as:

$$\bar{e}_\alpha = \frac{e_\alpha}{\bar{c}} \begin{cases} 0 & \alpha = 0, \\ \left\{ \cos \left[ (\alpha - 1) \frac{\pi}{2} \right], \sin \left[ (\alpha - 1) \frac{\pi}{2} \right] \right\} & \alpha = 1, 2, 3, 4, \\ \sqrt{2} \left\{ \cos \left[ (2\alpha - 1) \frac{\pi}{4} \right], \sin \left[ (2\alpha - 1) \frac{\pi}{4} \right] \right\} & \alpha = 5, 6, 7, 8, \\ 2 \left\{ \cos \left[ (\alpha - 9) \frac{\pi}{2} \right], \sin \left[ (\alpha - 9) \frac{\pi}{2} \right] \right\} & \alpha = 9, 10, 11, 12. \end{cases} \quad (1)$$

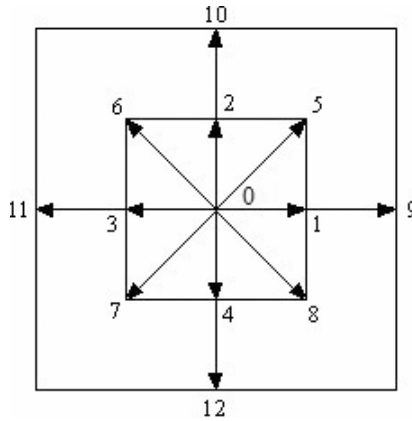


Fig. 1. Discrete velocities of the D2Q13 model.

Here  $\bar{c} = \sqrt{RT_c}$  is the characteristic speed of the lattice fluid, in which  $T_c$  is the characteristic temperature.

## 2.2. Coupled DDF model

The first DDF lattice Boltzmann model was devised by He *et al.*<sup>28</sup> The model introduced an internal energy density distribution function to simulate the temperature field. The macroscopic density and velocity fields are still simulated using the density distribution function. This model has attracted much attention since its emergence for its excellent numerical stability and adjustability of the Prandtl number. However, this model includes complicated gradient terms involving temporal and spatial derivatives of the macroscopic flow variables, which may introduce some additional errors and do harm to the numerical stability. Recently, Guo *et al.*<sup>29</sup> proposed another DDF model by introducing a total energy distribution function to replace the internal energy distribution function, but the model is a decoupling model in which the energy equation is decoupled from the momentum equation. In other words, the temperature field does not affect the flow field. It is known that, for compressible flows, the continuity equation is taken as the transport equation for the density while the energy equation is the transport equation for the temperature. The pressure can be obtained from the density and temperature by the thermal equation of state,  $p = p(\rho, T)$ . So we can naturally use the thermal equation of state to couple the two different distribution functions in the DDF model. In the coupled DDF lattice Boltzmann model, the evolution equation of density distribution function is given as follows:

$$\frac{\partial f_\alpha}{\partial t} + (e_\alpha \cdot \nabla) f_\alpha = -\frac{1}{\tau_f} (f_\alpha - f_\alpha^{\text{eq}}) \quad (\alpha = 1, 2, \dots, N). \quad (2)$$

The evolution equation of total energy distribution function is given as:

$$\frac{\partial h_\alpha}{\partial t} + (e_\alpha \cdot \nabla) h_\alpha = -\frac{1}{\tau_f} (h_\alpha - h_\alpha^{\text{eq}}) + \frac{1}{\tau_{hf}} (e_\alpha \cdot u) (f_\alpha - f_\alpha^{\text{eq}}), \quad (3)$$

where  $f_\alpha$  and  $h_\alpha$  are the density distribution function and the total energy distribution function, respectively;  $f_\alpha^{\text{eq}}$  and  $h_\alpha^{\text{eq}}$  are the equilibrium density distribution function, and the equilibrium total energy distribution function, respectively, whose specific expressions can be found in Refs. 4 and 6;  $\tau_f$  is the density relaxation time,  $\tau_h$  is the total energy relaxation time and  $\tau_{hf} = \tau_h \tau_f / (\tau_f - \tau_h)$ . The macroscopic variables are defined as:

$$\rho = \sum_\alpha f_\alpha^{\text{eq}}, \quad (4a)$$

$$\rho u_i = \sum_\alpha f_\alpha^{\text{eq}} e_{\alpha i}, \quad (4b)$$

$$T = \frac{2}{bR_g} \left( \sum_{\alpha} h_{\alpha}^{\text{eq}} - \frac{u^2}{2} \right), \quad (4c)$$

$$p = \rho R_g T, \quad (4d)$$

where  $p$ ,  $\rho$ ,  $T$  are macroscopic pressure, density, temperature, respectively;  $R_g$  is the specific gas constant;  $b$  is a constant, which is related to specific-heat ratio  $\gamma = (b + 2)/b$ .

### 2.3. Finite-difference scheme

To solve the hyperbolic equations (2) and (3), an implicit–explicit FDLBM, which consists of the implicit–explicit Runge–Kutta schemes in time discretization and WENO scheme in space discretization, is adopted.

#### 2.3.1. Time discretization

Implicit–explicit Runge–Kutta schemes are efficient in time discretization. The implicit–explicit expression of density distribution function is given as follows:

$$f_{\alpha}^{(J)} = \frac{f_{\alpha}^t - \delta t \sum_{k=1}^{J-1} \tilde{m}_{Jk} (e_{\alpha} \cdot \nabla f_{\alpha}^{(k)}) + \delta t \sum_{k=1}^{J-1} m_{Jk} \frac{f_{\alpha}^{\text{eq}(k)} - f_{\alpha}^{(k)}}{\tau_f^{(k)}} + \frac{\delta t}{\tau_f^{(J)}} m_{JJ} f_{\alpha}^{\text{eq}(J)}}{1 + \frac{\delta t}{\tau_f^{(J)}} m_{JJ}}, \quad (5)$$

where here  $f_{\alpha}^{(k)}$ ,  $f_{\alpha}^{\text{eq}(k)}$  and  $\tau_f^{(k)}$  are the  $k$ th-stage density distribution function, local equilibrium distribution function and relaxation time. The two  $r \times r$  matrices  $\tilde{M} = [\tilde{m}_{Jk}]$  ( $\tilde{m}_{Jk} = 0$  for  $k \geq J$ ) and  $M = [m_{Jk}]$  ( $m_{Jk} = 0$  for  $k > J$ ) characterize the implicit–explicit Runge–Kutta schemes.<sup>45</sup> Similarly, the implicit–explicit expression of internal energy distribution function is as follows:

$$h_{\alpha}^{(J)} = \frac{h_{\alpha}^t - \delta t \sum_{k=1}^{J-1} \tilde{m}_{Jk} (e_{\alpha} \cdot \nabla h_{\alpha}^{(k)}) - \delta t \sum_{k=1}^J m_{Jk} (e_{\alpha} \cdot u^{(k)}) \frac{f_{\alpha}^{\text{eq}(k)} - f_{\alpha}^{(k)}}{\tau_{hf}^{(k)}} + \delta t \sum_{k=1}^{J-1} m_{Jk} \frac{h_{\alpha}^{\text{eq}(k)} - h_{\alpha}^{(k)}}{\tau_h^{(k)}} + \frac{\delta t}{\tau_h^{(J)}} m_{JJ} h_{\alpha}^{\text{eq}(k)}}{1 + \frac{\Delta t}{\tau_h^{(J)}} m_{JJ}}. \quad (6)$$

#### 2.3.2. Space discretization

Consider the  $x$  component of the convection terms  $e_{\alpha} \cdot \nabla f_{\alpha}$  and  $e_{\alpha} \cdot \nabla h_{\alpha}$  in Eqs. (2) and (3),  $e_{\alpha} \cdot \nabla f_{\alpha}$  is described as:

$$\frac{\partial(e_{\alpha x} f_{\alpha})}{\partial x} = \frac{1}{\Delta x} (\hat{F}_{\alpha, i+1/2, j} - \hat{F}_{\alpha, i-1/2, j}). \quad (7)$$

In WENO scheme, the definition of the numerical flux  $\widehat{F}_{\alpha,i+1/2,j}$  is given as:

$$\widehat{F}_{\alpha,i+1/2,j} = \omega_0 \widehat{F}_{\alpha,i+1/2,j}^0 + \omega_1 \widehat{F}_{\alpha,i+1/2,j}^1 + \omega_2 \widehat{F}_{\alpha,i+1/2,j}^2. \quad (8)$$

Under the condition  $e_{\alpha x} \geq 0$ , three third-order fluxes on three different stencils  $\widehat{F}_{\alpha,i+1/2,j}^q (q = 1, 2, 3)$  are given as:

$$\widehat{F}_{\alpha,i+1/2,j}^0 = \frac{1}{3} F_{\alpha,i-2,j} - \frac{7}{6} F_{\alpha,i-1,j} + \frac{11}{6} F_{\alpha,i,j}, \quad (9a)$$

$$\widehat{F}_{\alpha,i+1/2,j}^1 = -\frac{1}{6} F_{\alpha,i-1,j} + \frac{5}{6} F_{\alpha,i,j} + \frac{1}{3} F_{\alpha,i+1,j}, \quad (9b)$$

$$\widehat{F}_{\alpha,i+1/2,j}^2 = \frac{1}{3} F_{\alpha,i,j} + \frac{5}{6} F_{\alpha,i+1,j} - \frac{1}{6} F_{\alpha,i+2,j}, \quad (9c)$$

where  $F_{\alpha,i,j} = e_{\alpha x} f_{\alpha,i,j}$ . The detailed analysis of  $\omega_k$  is given in Sec. 3. Similarly, under the condition  $e_{\alpha x} < 0$ , a mirror image procedure (with respect to  $i + 1/2$ ) of Eq. (9) can be carried out. For two-dimensional problems, these schemes should be applied in both  $x$ - and  $y$ -directions.

### 3. Analysis and Improvement of FDLBM

The WENO scheme is one of the most popular finite-difference methods. But a detailed analysis reveals that the version of this scheme implemented by Jiang and Shu<sup>46</sup> is only third-order accurate at critical points.<sup>47</sup> According to the analysis of the WENO scheme, a new smoothness indicator is devised to improve the order of convergence.

#### 3.1. Weighted method of WENO

The WENO scheme is an improvement on the essentially nonoscillatory (ENO) scheme, and it uses a convex combination of all candidate stencils instead of just one as in the original ENO scheme. From Eq. (8), the polynomial approximation  $\widehat{f}_{\alpha,i+1/2,j}$  is built through the convex combination of the interpolated values  $\widehat{f}_{\alpha,i+1/2,j}^k$  in WENO scheme. To describe conveniently,  $F$  is replaced by  $f$  in this section.

Consider a uniform grid defined by the points  $x_i = i\Delta x$ ,  $i = 0, \dots, N$ , which are also called cell centers, with cell boundaries given by  $x_{i\pm 1/2} = x_i + \Delta x/2$ , where  $\Delta x$  is the uniform grid spacing. Following Liu and Osher,<sup>48</sup> the numerical flux function  $h(x)$  is defined according to

$$f(x) = \frac{1}{\Delta x} \int_{x-\Delta x/2}^{x+\Delta x/2} h(\xi) d\xi. \quad (10)$$

Hence the spatial derivative  $\partial(e_{\alpha x} f_{\alpha})/\partial x$  can be exactly approximated by a conservative finite difference formula at the cell boundaries

$$\frac{\partial(e_{\alpha x} f_{\alpha})}{\partial x} = \frac{1}{\Delta x} [h_{i+1/2} - h_{i-1/2}], \tag{11}$$

where  $h_{i\pm 1/2} = h(x_{i\pm 1/2})$ .

By approximating  $h(x)$  in Eq. (10), these approximations of  $h(x)$  are denoted by  $\hat{f}(x)$  and the spatial derivative is approximated by

$$\frac{\partial(e_{\alpha x} f_{\alpha})}{\partial x} \approx \frac{1}{\Delta x} [\hat{f}_{i+1/2} - \hat{f}_{i-1/2}]. \tag{12}$$

The above equation is identical to Eq. (7).

The classical fifth-order WENO scheme uses a 5-points stencil, named  $S^5$ , which is subdivided into three 3-points stencils  $\{S_0, S_1, S_2\}$ , as shown in Fig. 2. The numerical flux  $\hat{f}_{i\pm 1/2}$  is rebuilt by the third degree polynomial as follows:

$$\hat{f}_{i\pm 1/2} = \sum_{k=0}^2 \omega_k \hat{f}^k(x_{i\pm 1/2}), \tag{13}$$

where  $\hat{f}^k(x_{i\pm 1/2}) = \hat{f}_{i\pm 1/2}^k = \sum_{j=0}^2 c_{kj} f_{i-k+j}$ ,  $i = 0, \dots, N$ . It can be shown by Taylor series expansion of Eq. (13) as follows:

$$\hat{f}_{i\pm 1/2}^k = h_{i\pm 1/2} + A_k \Delta x^3 + O(\Delta x^4). \tag{14}$$

The weights in Eq. (8) are defined as

$$\omega_k = \frac{\alpha_k}{\sum_{l=0}^2 \alpha_l}, \tag{15}$$

$$\alpha_k = \frac{d_k}{(\beta_k + \varepsilon)^2}, \tag{16}$$

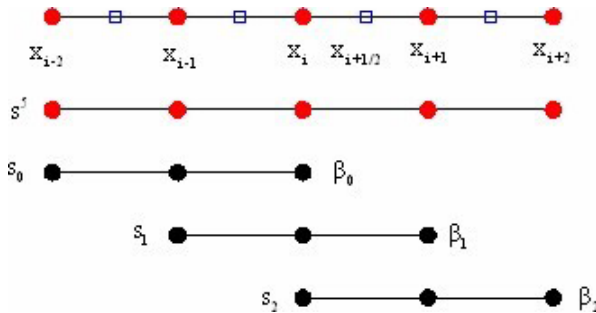


Fig. 2. (Color online) The computational uniform grid  $x_i$  and the 5-points stencil  $S^5$ , composed of three 3-points stencils  $S_0, S_1, S_2$ , used for the fifth-order WENO reconstruction.

where the coefficient  $d_0 = 1/10$ ,  $d_1 = 3/5$ ,  $d_2 = 3/10$  are the ideal weights,  $\beta_k$  is smooth indicator.

**3.2. Analysis and improvement of the smoothness indicator**

Smoothness indicator<sup>47</sup> is defined as:

$$\beta_k = \sum_{l=1}^2 \Delta x^{2l-1} \int_{x_{i-1/2}}^{x_{i+1/2}} \left( \frac{d^l}{dx^l} \widehat{f}^k(x) \right)^2 dx. \tag{17}$$

A polynomial form is postulated  $\widehat{f}^k = b_0 + b_1x + b_2x^2$  (see Ref. 47) and the integral is simplified as,

$$\beta_k = b_1^2 \Delta x^2 + \frac{13b_2^2 \Delta x^4}{3}. \tag{18}$$

According to Ref. 47, substitution  $b_1$  and  $b_2$  into Eq. (18) gives

$$\beta_0 = \frac{13}{12} \underbrace{(f_{i-2} - 2f_{i-1} + f_i)^2}_{\Delta x^2(f_i'' + O(\Delta x))} + \frac{1}{4} \underbrace{(f_{i-2} - 4f_{i-1} + 3f_i)^2}_{2\Delta x(f_i' + O(\Delta x^2))}, \tag{19a}$$

$$\beta_1 = \frac{13}{12} \underbrace{(f_{i-1} - 2f_i + f_{i+1})^2}_{\Delta x^2(f_i'' + O(\Delta x^2))} + \frac{1}{4} \underbrace{(f_{i-1} - f_{i+1})^2}_{2\Delta x f_i' + O(\Delta x^2)}, \tag{19b}$$

$$\beta_2 = \frac{13}{12} \underbrace{(f_i - 2f_{i+1} + f_{i+2})^2}_{\Delta x^2(f_i'' + O(\Delta x))} + \frac{1}{4} \underbrace{(3f_i - 4f_{i+1} + f_{i+2})^2}_{-2\Delta x(f_i' + O(\Delta x^2))}. \tag{19c}$$

The Taylor series expansions of Eqs. (19) give:

$$\begin{aligned} \beta_0 &= f_i'^2 \Delta x^2 + \left( \frac{13}{12} f_i''^2 - \frac{2}{3} f_i' f_i''' \right) \Delta x^4 \\ &\quad - \left( \frac{13}{6} f_i'' f_i''' - \frac{1}{2} f_i' f_i^{(4)} \right) \Delta x^5 + O(\Delta x^6), \end{aligned} \tag{20a}$$

$$\beta_1 = f_i'^2 \Delta x^2 + \left( \frac{13}{12} f_i''^2 + \frac{1}{3} f_i' f_i''' \right) \Delta x^4 + O(\Delta x^6), \tag{20b}$$

$$\begin{aligned} \beta_2 &= f_i'^2 \Delta x^2 + \left( \frac{13}{12} f_i''^2 - \frac{2}{3} f_i' f_i''' \right) \Delta x^4 \\ &\quad + \left( \frac{13}{6} f_i'' f_i''' - \frac{1}{2} f_i' f_i^{(4)} \right) \Delta x^5 + O(\Delta x^6). \end{aligned} \tag{20c}$$

With the above equations, it is assumed that the smoothness indicator can be written as:

$$\beta_k = D(1 + O(\Delta x^2)) \quad k = 0, 1, 2, \tag{21}$$

where  $D$  is a nonzero constant.

Table 1. Orders comparison of  $\beta_k$ .

$f' \neq 0$	$f' = 0$
$\beta_0 = (f' \Delta x)^2(1 + O(\Delta x^2))$	$\beta_0 = \frac{13}{12}(f'' \Delta x^2)^2(1 + O(\Delta x))$
$\beta_1 = (f' \Delta x)^2(1 + O(\Delta x^2))$	$\beta_1 = \frac{13}{12}(f'' \Delta x^2)^2(1 + O(\Delta x^2))$
$\beta_2 = (f' \Delta x)^2(1 + O(\Delta x^2))$	$\beta_2 = \frac{13}{12}(f'' \Delta x^2)^2(1 + O(\Delta x))$

Substituting Eq. (21) into Eqs. (15) and (16) gives:

$$\alpha_k = \frac{d_k}{(D(1 + O(\Delta x^2)))^2} = \frac{d_k}{D^2}(1 + O(\Delta x^2)), \quad (22)$$

$$\omega_k = d_k + O(\Delta x^2). \quad (23)$$

Equation (23) satisfies one of the necessary and sufficient constraints for fifth-order convergence.<sup>47</sup> But if the first derivative vanishes ( $f' = 0$ ),  $\beta_0$  and  $\beta_2$  cannot satisfy Eq. (23), as shown in Table 1.

In order to improve the order of convergence, a new smoothness indicator which uses the whole 5-points stencil  $S^5$  is devised. We denote it by  $\tau_G$  and it is simply defined as the absolute difference between  $\beta_0$  and  $\beta_2$  at  $x_i$ :

$$\tau_G = |\beta_0 - \beta_2|. \quad (24)$$

From Eq. (19) it can be seen that the truncation error of  $\tau_G$  is

$$\tau_G = \frac{13}{3}|f''_i f'''_i| \Delta x^5 + O(\Delta x^6). \quad (25)$$

Now the new smoothness indicator  $\beta_k^G$  is defined as

$$\beta_k^G = \left( \frac{\beta_k + \varepsilon}{\beta_k + \tau_G + \varepsilon} \right), \quad k = 0, 1, 2. \quad (26)$$

The new WENO weights  $\omega_k^G$  are given as,

$$\omega_k^G = \frac{\alpha_k^G}{\sum_{l=0}^2 \alpha_l^G}, \quad (27)$$

$$\alpha_k^G = \frac{d_k}{\beta_k^G} = d_k \left( 1 + \frac{\tau_G}{\beta_k + \varepsilon} \right) \quad k = 0, 1, 2. \quad (28)$$

Then the convergence order can be obtained:

$$\left( 1 + \frac{\tau_G}{\beta_k^G} \right) = 1 + O(\Delta x^3), \quad (29)$$

$$\omega_k^G = d_k + O(\Delta x^3). \quad (30)$$

**3.3. The analysis of convergence**

Adding and subtracting  $\sum_{k=0}^2 d_k \widehat{f}^k(x_{i\pm 1/2})$  from Eq. (13) gives

$$\begin{aligned} \widehat{f}_{i\pm 1/2} &= \sum_{k=0}^2 d_k \widehat{f}_{i\pm 1/2}^k + \sum_{k=0}^2 (\omega_k^\pm - d_k) \widehat{f}_{i\pm 1/2}^k \\ &= [h_{i\pm 1/2} + B^\pm \Delta x^5 + O(\Delta x^6)] + \sum_{k=0}^2 (\omega_k^\pm - d_k) \widehat{f}_{i\pm 1/2}^k \\ &= h_{i\pm 1/2} \sum_{k=0}^2 (\omega_k^\pm - d_k) + \Delta x^3 \sum_{k=0}^2 A_k (\omega_k^\pm - d_k) + \sum_{k=0}^2 (\omega_k^\pm - d_k) O(\Delta x^4). \end{aligned} \tag{31}$$

Substituting the results above at a finite difference formula for the polynomial approximation  $\widehat{f}_{i\pm 1/2}$

$$\begin{aligned} \frac{\widehat{f}_{i+1/2} - \widehat{f}_{i-1/2}}{\Delta x} &= \frac{h_{i+1/2} - h_{i-1/2}}{\Delta x} + O(\Delta x^5) \\ &\quad + \frac{\sum_{k=0}^2 (\omega_k^+ - d_k) \widehat{f}_{i+1/2}^k - \sum_{k=0}^2 (\omega_k^- - d_k) \widehat{f}_{i-1/2}^k}{\Delta x} \\ &= f'(x_i) + O(\Delta x^5) + \left[ \frac{h_{i+1/2} \sum_{k=0}^2 (\omega_k^+ - d_k) - h_{i-1/2} \sum_{k=0}^2 (\omega_k^- - d_k)}{\Delta x} \right] \\ &\quad + \Delta x^2 \sum_{k=0}^2 A_k (\omega_k^+ - \omega_k^-) + \left[ \sum_{k=0}^2 (\omega_k^+ - d_k) - \sum_{k=0}^2 (\omega_k^- - d_k) \right] O(\Delta x^3). \end{aligned} \tag{32}$$

The order of the improving WENO scheme is given as

$$s = \min(5, s_1 + 2, s_2 + 3), \tag{33}$$

where

$$\sum_{k=0}^2 A_k (\omega_k^+ - \omega_k^-) = O(\Delta x^{s_1}), \tag{34}$$

$$\omega_k^\pm - d_k = O(\Delta x^{s_2}). \tag{35}$$

From Eq. (28) it is easily found that

$$\alpha_k^G - d_k = d_k \frac{\tau_G}{\beta_k^G + \varepsilon}, \tag{36}$$

$$\omega_k^G - d_k = O\left(\frac{\tau_G}{\beta_k^G + \varepsilon}\right). \tag{37}$$

For  $s_1$ , Eq. (34) can be expanded as<sup>49</sup>

$$\sum_{k=0}^2 A_k (\omega_k^{G^+} - \omega_k^{G^-}) = \Omega^+ - \Omega^- = \frac{N^+ D^- - N^- D^+}{D^+ D^-}, \quad (38)$$

where

$$\Omega^\pm = \sum_{k=0}^2 A_k \omega_k^{G^\pm} = \frac{\sum_{k=0}^2 F_k^\pm(A_k)}{1 + \sum_{k=0}^2 F_k^\pm(1)} \quad \text{with} \quad F_k^\pm(\gamma) = \tau_G^\pm \gamma \frac{d_k}{\beta_k}, \quad (39)$$

and

$$N^\pm = \tau_G^\pm \left( \prod_{k=0}^2 \beta_k^{G^\pm} \right) \sum_{k=0}^2 \frac{A_k d_k}{\beta_k^{G^\pm}}, \quad D^\pm = \prod_{k=0}^2 \beta_k^{G^\pm} + \tau_G^\pm \left( \prod_{k=0}^2 \beta_k^{G^\pm} \right) \sum_{k=0}^2 \frac{d_k}{\beta_k^{G^\pm}}. \quad (40)$$

In the above derivation, we have used  $\sum_{k=0}^2 A_k d_k = 0$  and  $\sum_{k=0}^2 d_k = 1$ .

If  $f' \neq 0$ ,  $s_1 = 6$ ,  $s_2 = 3$ ; If  $f' = 0$ ,  $s_1 = 2$ ,  $s_2 = 1$ . Therefore, if the first derivatives vanishes, the order of the WENO-G scheme is attained order  $s = 4$ , improving over the classical WENO which attains only order 3, or  $s = 5$ .

#### 4. Improved Finite-Difference Lattice Boltzmann Scheme for Compressible Flows

In Sec. 3, an improved finite-difference lattice Boltzmann method (FDLBM-G) is developed. In this section, as preliminary tests, numerical simulation is performed for the Riemann problem. The flow of the Riemann problem includes a shock wave, contact surface and an expansion wave. Hence, it is a wonderful model problem that can be used to study the performance of the numerical schemes in simulating compressible flows. Two different cases are considered in this study.

**Case 1.** Sod shock tube with the initial conditions given as

$$\begin{cases} (\rho/\rho_0, u_x/u, p/p_0) = (1, 0, 1), & 0 < x/L_0 \leq 1/2, \\ (\rho/\rho_0, u_x/u, p/p_0) = (0.125, 0, 0.1), & 1/2 < x/L_0 < 1, \end{cases} \quad (41)$$

where  $L_0$  is the reference length and  $L_0 = 2m$ ;  $\rho_0$ ,  $u_0 = \sqrt{R_g T_0}$ ,  $f_\alpha = f_\alpha^{\text{eq}}$  and  $T_0$  are reference density, reference velocity, reference pressure and reference temperature, respectively. The characteristic time of system is defined as  $t_0 = L_0/u_0$ . The fluid is assumed as the ideal gas with  $\rho_0 = 1.165 \text{ kg/m}^3$ ,  $R_g = 287 \text{ J/(kg} \cdot \text{K)}$ ,  $T_0 = 303 \text{ K}$  and  $\mu = 1.86 \times 10^{-5} \text{ kg/(m} \cdot \text{s)}$ . The specific-heat ratio is set to be 1.4 with  $b = 5$  and the Prandtl number is set to be 0.71. The mesh is specified by setting  $N_x \times N_y = 400 \times 5$ , where  $N_x$  and  $N_y$  are the lattice numbers along the  $x$  and  $y$  directions, respectively. On the boundary nodes in the  $x$ -direction,  $f_\alpha = f_\alpha^{\text{eq}}$  is set before the disturbance reaches the two ends. In the  $y$ -direction, the periodic boundary condition is adopted.

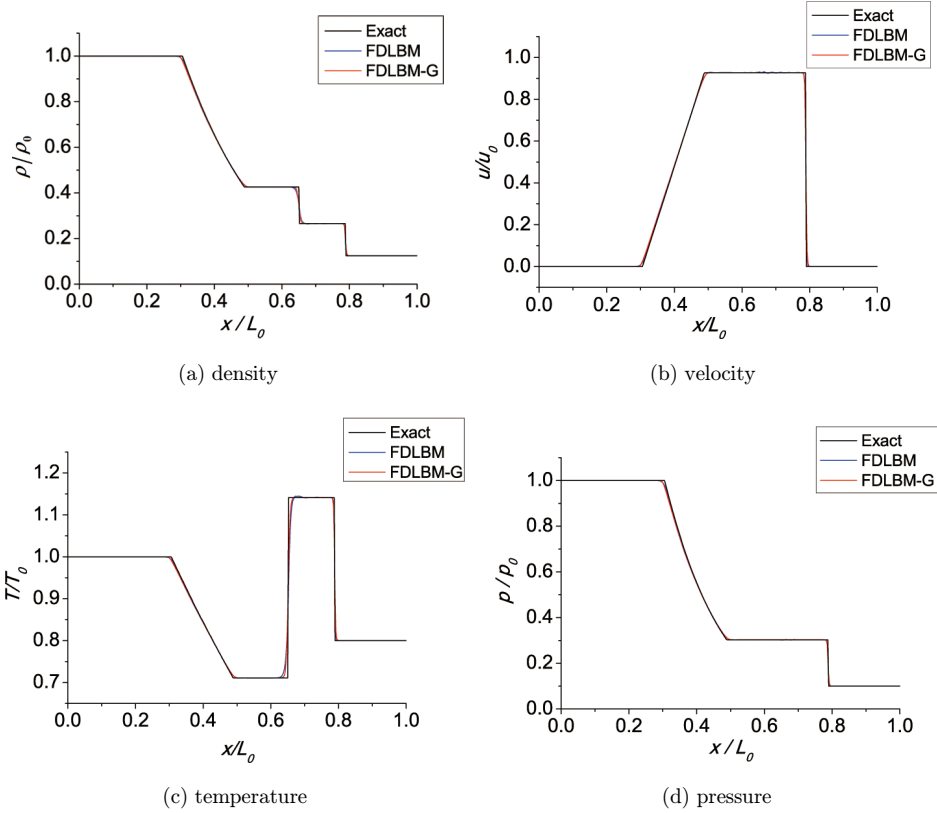


Fig. 3. (Color online) Comparisons between two numerical and exact solutions for sod shock tube.

The predicted profiles of the velocity, temperature, density and pressure at  $t = 0.1644t_0$  for the sod shock tube are presented in Fig. 3. The numerical results of the improved scheme are found to be in excellent agreement with the analytical ones and better than those of the previous scheme. Although the accuracy is improved, it can be observed from Fig. 3 that there are some minor discrepancies between the two numerical and exact solutions on the position of the contact discontinuities. The local details of the temperature and density near the shock wave are shown in Fig. 4.

**Case 2.** Strong shock wave with the initial conditions given as,

$$\begin{cases} (\rho/\rho_0, u_x/u, p/p_0) = (1, 0, 1000), & 0 < x/L_0 \leq 1/2, \\ (\rho/\rho_0, u_x/u, p/p_0) = (1, 0, 0.01), & 1/2 < x/L_0 < 1. \end{cases} \quad (42)$$

The strong shock wave problem, which has an extremely large pressure ratio, 100 000, is a very challenging problem for numerical schemes. For this test, we set  $T_c = 1000T_0$ . The profiles of the velocity, temperature density and pressure at  $t = 0.012t_0$  are shown in Fig. 5. To sum up, the numerical results agree well with the analytical results. However, there are some noticeable difference between FDLBM

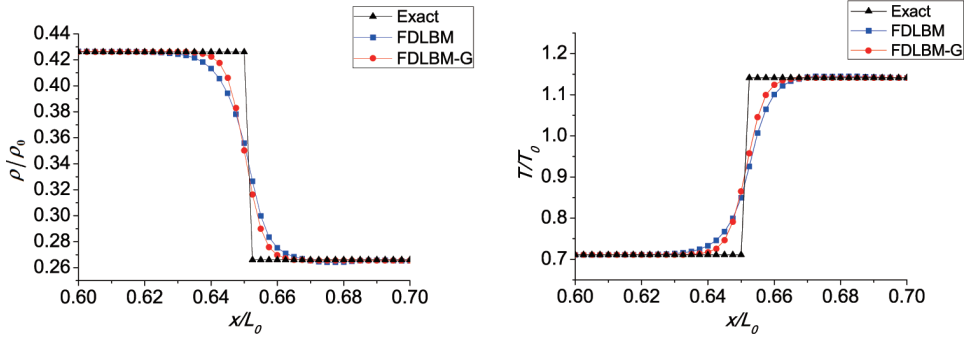


Fig. 4. (Color online) Local details of the temperature and density near the shock wave in 0.6–0.7.

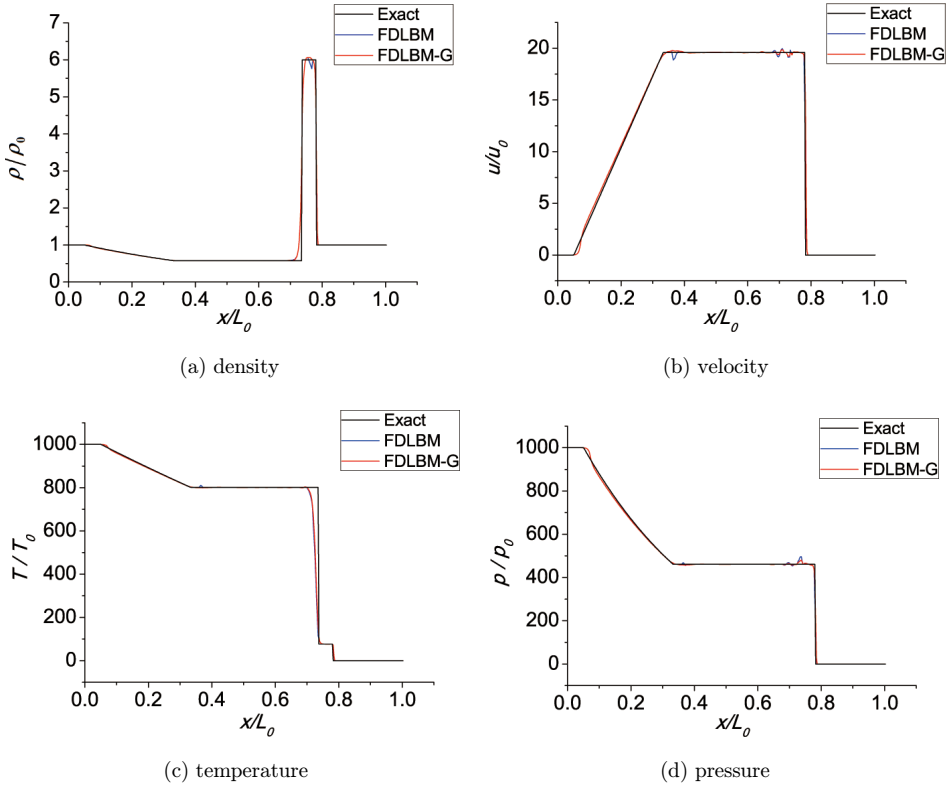


Fig. 5. (Color online) Comparisons between two numerical and exact solutions for sod shock tube.

Table 2. Relative global errors of the density, velocity, temperature and pressure.

	Case 1		Case 2	
	FDLBM	FDLBM-G	FDLBM	FDLBM-G
$\rho$	$1.24 \times 10^{-4}$	$1.12 \times 10^{-4}$	$1.93 \times 10^{-3}$	$1.84 \times 10^{-3}$
$u$	$1.47 \times 10^{-3}$	$1.13 \times 10^{-3}$	$3.02 \times 10^{-2}$	$1.89 \times 10^{-2}$
$T$	$3.58 \times 10^{-4}$	$2.99 \times 10^{-4}$	$6.94 \times 10^{-3}$	$5.63 \times 10^{-3}$
$p$	$1.00 \times 10^{-4}$	$8.7 \times 10^{-5}$	$5.42 \times 10^{-4}$	$4.45 \times 10^{-4}$

and FDLBM-G near the shock wave, expansion wave and contact surface. According to the results of two cases, it is shown that FDLBM-G has less dissipation and more accurate than FDLBM.

To enable a comparison between the improved scheme and the previous scheme, the relative global errors of the density, velocity, temperature and pressure are measured. The results are given in Table 2. The relative global error<sup>50</sup> is defined by

$$\text{Error} = \frac{\sum_{i,j} (\phi_{i,j} - \bar{\phi}_{i,j})^2}{\sum_{i,j} \bar{\phi}_{i,j}^2}, \tag{43}$$

where  $\bar{\phi}_{i,j}$  is the analytical solution of the density, velocity, temperature and pressure;  $\phi_{i,j}$  is the numerical solution of the density, velocity, temperature and pressure for the improving and previous scheme.

Table 2 shows that the relative global errors predicted by the scheme proposed in this paper are smaller than the errors of the previous finite-difference lattice Boltzmann scheme. Moreover, it is seen that the numerical results confirm the theoretical analysis.

### 5. Conclusions

In this paper, the space discretization of the finite-difference lattice Boltzmann is analyzed and a new smoothness indicator is proposed. The new smoothness provides a convex combination of stencils with enhanced order of convergence and less dissipation at shocks. The improved scheme together with the coupled DDF lattice Boltzmann model is used to simulate compressible flows. Numerical results of sod shock tube and strong shock wave show that the improved FDLBM confirms the theoretical analysis. Numerical results demonstrated that FDLBM-G has less dissipation and more accurate than FDLBM.

### Acknowledgments

We warmly thank Zhaoli Guo, Qing Li, Yong Wang, Fangbao Tian, Yanbiao Gan for helpful discussions. Suggestions from the anonymous referee are gratefully acknowledged.

## References

1. S. Chen and G. Doolen, *Ann. Rev. Fluid Mech.* **30**, 329 (1998).
2. S. Succi, *The Lattice Boltzmann Equation for Fluid Dynamics and Beyond* (Clarendon Press, Oxford, 2001).
3. D. Yu, R. Mei, L. S. Luo and W. Shyy, *Prog. Aerospace. Sci.* **39**, 329 (2003).
4. Y. L. He, Y. Wang and Q. Li, *Lattice Boltzmann Method: Theory and Applications* (Science Press, Beijing, 2009).
5. Z. L. Guo and C. G. Zheng, *Theory and Applications of Lattice Boltzmann Method* (Science Press, Beijing, 2009).
6. Q. Li, Y. L. He, Y. Wang and W.Q. Tao, *Phys. Rev. E* **76**, 056705 (2007).
7. K. Xu, *J Stat. Phys.* **81**, 147 (1995).
8. W. Yu and X. Zhang, *J. Appl. Mech* **77**, 051406 (2010).
9. Y. H. Qian, *J. Sci. Comput.* **8**, 231 (1993).
10. F. J. Alexander, S. Chen and J. D. Sterling. *Phys. Rev. E* **47**, 2249 (1993).
11. Y. Chen, H. Ohashi and M. Akiyama, *Phys. Rev. E* **50**, 2776 (1994).
12. Y. Chen, H. Ohashi and M. Akiyama, *J. Sci. Comput.* **13**, 218 (1997).
13. M. Watari and M. Tsutahara, *Phys. Rev. E* **67**, 036306 (2003).
14. X. Pan, A. Xu, G. Zhang and S. Jiang, *Int. J. Mod. Phys. C* **18**, 1747 (2007).
15. Y. Gan, A. Xu, G. Zhang, X. Yu and Y. Li, *Phys. A* **387**, 1721 (2008).
16. Y. Gan, A. Xu, G. Zhang and Y. Li, *Phys. Rev. E* **83**, 056704 (2011).
17. Y. Gan, A. Xu, G. Zhang, Y. Li and H. Li, *Phys. Rev. E* **84**, 046715 (2011).
18. S. Hu, G. Yan and W. Shi, *Acta Mech. Sin.* **13**, 218 (1997).
19. G. Yan, Y. Chen and S. Hu, *Phys. Rev. E* **59**, 454 (1999).
20. K. Qu, C. Shu and Y. T. Chew, *Phys. Rev. E* **75**, 036706 (2007).
21. C. Sun, *Phys. Rev. E* **58**, 7283 (1998).
22. C. Sun, *Phys. Rev. E* **61**, 2645 (2000).
23. C. Sun, *J. Comput. Phys.* **161**, 70 (2000).
24. F. Chen, A. Xu, G. Zhang, Y. Li and S. Succi, *Europhys. Lett.* **90**, 54003 (2010).
25. F. Chen, A. Xu, G. Zhang and Y. Li, *Phys. Lett. A* **375**, 2129 (2011).
26. F. Chen, A. Xu, G. Zhang and Y. Li, *Commun. Theor. Phys.* **55**, 325 (2011).
27. F. Chen, A. Xu, G. Zhang and Y. Li, *Theor. Appl. Mech. Lett.* **1**, 052004 (2011).
28. X. He, S. Chen and G. Doolen, *J. Comput. Phys.* **146**, 282 (1998).
29. Z. Guo, C. Zheng and B. Shi, *Phys. Rev. E* **75**, 036704 (2007).
30. M. B. Reider and J. D. Sterling, *Comput. Fluids* **24**, 459 (1995).
31. N. Cao, S. Chen, J. Shi and D. Martinez, *Phys. Rev. E* **55**, R21 (1997).
32. R. Mei and W. Shyy, *J. Comput. Phys.* **143**, 426 (1998).
33. J. Tolke, M. Krafczyk, M. Schulz, E. Rank and R. Berrios, *Int. J. Mod. Phys. C* **9**, 1143 (1998).
34. Z. Guo and T. S. Zhao, *Phys. Rev. E* **71**, 066709 (2003).
35. Q. Li, Y. He and Y. Gao, *Int. J. Mod. Phys. C* **19**, 1581 (2008).
36. M. Watari and M. Tsutahara, *Phys. Rev. E* **67**, 036306 (2003).
37. I. Kim, W. B. Lindquist and W. B. Durham, *Phys. Rev. E* **67**, 046708 (2003).
38. V. Sofonea *et al.*, *Phys. Rev. E* **70**, 046702 (2004).
39. T. Kataoka and M. Tsutahara, *Phys. Rev. E* **69**, 056702 (2004).
40. T. Kataoka and M. Tsutahara, *Phys. Rev. E* **69**, 035701 (2004).
41. W. Shi, W. Mei and R. Mei, *Numer. Heat Transf. B* **40**, 1 (2001).
42. Y. Wang, Y. He, T. Zhao, G. Tang and W. Tao, *Int. J. Mod. Phys. C* **18**, 1961 (2007).
43. Z. Guo and T. S. Zhao, *Phys. Rev. E* **71**, 026701 (2005).
44. A. Xu, *Phys. Rev. E* **71**, 066706 (2005).
45. S. Pieraccini and G. Puppo, *J. Sci. Comput.* **32**, 1 (2007).

46. G. S. Jiang and C. W. Shu, *J. Comput. Phys.* **126**, 202 (1996).
47. H. Henrick, D. Aslam and M. Powers, *J. Comput. Phys.* **207**, 542 (2007).
48. X. Liu, S. Osher and T. Chan, *J. Comput. Phys.* **115**, 200 (1994).
49. R. Borges, M. Carmona, B. Costa and W. Don, *J. Comput. Phys.* **227**, 3191 (2008).
50. Z. Guo, C. Zheng and N. Wang, *J. Comput. Phys.* **165**, 288 (1996).